Measurements and modeling of electric-dipole-forbidden $2p_{1/2}$-$2p_{3/2}$ transitions in fluorinelike U^{81+} through berylliumlike U^{88+}

P. Beiersdorfer, A. L. Osterheld, and S. R. Elliott*
Department of Physics and Space Technology, Lawrence Livermore National Laboratory, Livermore, California 94551
(Received 1 May 1998)

We report the observation of electric-dipole-forbidden $2p_{1/2}$-$2p_{3/2}$ transitions in berylliumlike, boronlike, carbonlike, nitrogenlike, oxygenlike, and fluorinelike uranium. Our measurement identified nine magnetic dipole transitions, as well as one strong electric quadrupole transition in carbonlike U^{86+} that has not been observed in lower-Z ions because of collisional quenching. The measurement was carried out with a high-resolution crystal spectrometer, and an accuracy as good as 35 ppm was obtained in the determination of the transition energies. The transitions are significantly less affected by quantum electrodynamical effects than analogous electric-dipole-allowed transitions in these ions. The data thus provide benchmarks for theoretical approaches of electron-electron correlation effects in the high-Z limit $Z\alpha \approx 1$ that complement earlier measurements of $2s$-$2p$ transitions in such highly charged ions. The accuracy of the present measurements, however, was sufficient to determine the residual contributions from quantum electrodynamics (about 2 eV) with an accuracy of 5%, i.e., with an accuracy comparable to that of the best measurements of such contributions to the $1s$ ground level in hydrogenic U^{91+}. The contributions from quantum electrodynamics are in large part due to the vacuum polarization terms. The $2p_{1/2}$-$2p_{3/2}$ transition energies thus provide a handle for testing the accuracy of vacuum polarization terms nearly independent of the terms arising from the electron self energy. Results from collisional-radiative calculations are presented that show that the forbidden lines are almost exclusively produced by indirect processes, i.e., radiative cascades, radiative electron capture, and the ionization of $2p_{1/2}$ electrons. This is in stark contrast to the electric dipole-allowed transitions, which are mostly populated by direct electron-impact excitation. [S1050-2947(98)12209-6]

PACS number(s): 32.30.Rj, 12.20.Fv, 31.30.Jv, 32.70.Fw

I. INTRODUCTION

The structure of very highly charged ions has come under scrutiny only in the past few years, as appropriate sources of such ions were developed that enabled precise spectral measurements. One spectroscopic source of very highly charged ions is given by heavy-ion accelerators, which provide highly charged ions at strongly relativistic speeds. An alternate method, a high-energy electron-beam ion trap, provides stationary highly charged ions with low thermal energy. The utility of the latter method for performing accurate spectroscopic measurements was first demonstrated in a measurement of the contributions from quantum electrodynamics to electrons in the $2s$ subshell in Yb^{60+} [1]. The method now provides access to spectra as high as Cf^{96+} [2]. The main thrust of such measurements is to provide accurate atomic structure information to test the predictions of QED and relativity in very strong nuclear fields where $Z\alpha \approx 1$.

Measurements of the $2s$-$2p$ transitions in lithiumlike ions currently provide the most precise test of QED in strong nuclear fields. For example, measurements of the $2s_{1/2}$-$2p_{3/2}$ transitions in lithiumlike thorium and uranium yielded values of 4025.23 ± 0.14 and 4459.37 ± 0.21, respectively [3,4]. These measurements tested the respective net QED contributions of 36 and 39 eV to 0.4% and 0.5%, respectively. A measurement of the $2s_{1/2}$-$2p_{1/2}$ transition in lithiumlike uranium that yielded 280.59 ± 0.10 tested the net QED contribution to 0.2% [5]. The (2788.139 ± 0.039)-eV measurement of the $2s_{1/2}$-$2p_{3/2}$ transition in lithiumlike Bi^{80+} currently provides the most accurate measurement of the QED term, testing the net 26.3-eV contribution within 0.15% [6]. By contrast, the best determination of the QED contribution to the energy of the $1s$ in hydrogenlike uranium [7] inferred from measurements of the $1s$-$2p$ transition energies tests the theory only to within about 6%, i.e., with 40 times less accuracy.

Measurements with similar high accuracy as measurements of the $2s_{1/2}$-$2p_{3/2}$ transition in very highly charged lithiumlike ions have also been made for $2s_{1/2}$-$2p_{3/2}$ transitions in the neighboring charge states, i.e., in berylliumlike through neonlike uranium and thorium [4,8]. The energies of these transitions are affected by QED in ways similar to the lithiumlike transitions, and thus provide additional tests of the QED terms. Unlike the $2s$-$2p$ transitions in lithiumlike ions, these transitions are, however, significantly affected by correlation effects. Until recently, these correlation energies have prevented accurate calculations of the non-QED energies, and thus have precluded precise tests of the QED terms. For example, a comparison of the measured values with standard multiconfigurational Dirac-Fock calculations yielded differences as large as 8 eV [4,8]. A breakthrough was achieved when Johnson, Sapirstein, and Blundell [9] applied relativistic many-body perturbation theory (RMBPT) to the calculation of the Dirac energies of berylliumlike, carbonlike, fluorinelike, and neonlike uranium. The method they used was shown to be well suited to high-Z ions because of

*Present address: Nuclear Physics Laboratory, University of Washington, Seattle, WA 98195.

the rapid convergence of the $1/Z$ expansion that is part of the RMBPT method. Agreement with the measurements were achieved within about 0.5 eV for the lithiumlike, carbonlike, and fluorinelike transitions. An agreement within only 2 eV was found for the berylliumlike transition. Cheng and Chen [10] performed a large-scale relativistic configuration-interaction calculation to treat correlation effects accurately in berylliumlike uranium. Their calculation achieved agreement with the measurement within experimental uncertainties (0.21 eV). Similarly good agreement was found by Safronova, Johnson, and Safronova [11]. A newer calculation by Chen and Cheng [12], however, differs again from experiment by about 0.4 eV.

Because the $2s_{1/2}$-$2p_{3/2}$ transitions in berylliumlike through neonlike ions are affected by both QED and correlation effects, a comparison between measurements and calculations provides a test of the combination of both effects. To test the theories that predict the correlation energies, measurements are needed of transitions that are not as much affected by QED terms as the $2s_{1/2}$-$2p_{3/2}$ transitions. Moreover, such measurements must be of transitions in very high-Z ions because present theoretical approaches, such as RMBPT, converge best and are most reliable in the high-Z limit.

To aid the development of theoretical treatments of correlation effects in high-Z ions, we present a precise measurement of ten $2p_{1/2}$-$2p_{3/2}$ transitions in the six adjacent charge states berylliumlike U^{88+} through fluorinelike U^{83+}. Unlike the $2s_{1/2}$-$2p_{3/2}$ transitions, which are electric-dipole-allowed ($E1$) transitions, the $2p_{1/2}$-$2p_{3/2}$ transitions are electric-dipole-''forbidden'' transitions, i.e., they are transitions which have radiative rates significantly (many orders of magnitude) less than those of the $E1$ transitions. Nine of the observed transitions are magnetic-dipole ($M1$) transitions. One is an electric-quadrupole ($E2$) transition. Unlike $2s$ electrons, $2p$ electrons do not significantly penetrate the nucleus. The QED contributions for these transitions are thus substantially (almost an order of magnitude) less than those for the $2s_{1/2}$-$2p_{3/2}$ transitions. Our measurements are, therefore, complementary to our earlier measurements of the $2s_{1/2}$-$2p_{3/2}$ transitions [8] by providing benchmarks for testing theoretical approaches for calculating electron-electron correlation effects in the comparative absence of QED effects. The QED contributions to the $2p_{1/2}$-$2p_{3/2}$ transitions, however, by no means vanish. Given the high accuracy with which we have measured the transition energies of the forbidden transitions, the present measurements not only provide benchmarks for testing correlation effects but also for QED effects. In fact, the accuracy is sufficient, in principle, to test the QED terms affecting the $2p_{1/2}$-$2p_{3/2}$ transitions within about 5% and, therefore, comparable to the accuracy of the best measurement [7] of the QED contribution to the $1s$ level in hydrogenic uranium.

Earlier measurements of dipole-forbidden $2p_{1/2}$-$2p_{3/2}$ transitions extend to elements with atomic number Z as high as 42 [13–15]. For example, a set of nine $2p_{1/2}$-$2p_{3/2}$ $M1$ transitions in highly charged krypton ($Z=36$) was measured by Denne *et al.* on the Joint European Torus [14]. Their measurement provided the energies of one $M1$ transition in fluorinelike, two in oxygenlike, three in nitrogenlike, one in carbonlike, one in boronlike, and one in berylliumlike krypton. A recent study by Myrnäs *et al.* extended the observation of $2p_{1/2}$-$2p_{3/2}$ $M1$ decay in fluorinelike and boronlike ions to molybdenum ($Z=42$) [15]. The set of $M1$ transitions in uranium presented here more than doubles the atomic number of the ions for which such transitions have been measured. We are not aware of an earlier identification of $E2$ decay among $2p_{1/2}$-$2p_{3/2}$ transitions. These transitions decay slower than most $M1$ transitions, and are more likely to be collisionally quenched in low-Z ions. The identification of such a transition in our present study thus appears to be the only of its kind.

The radiative decay rates of the $M1$ and $E2$ transitions in uranium are 3–4 orders of magnitude less than those for the $E1$ transitions. However, they are in the range 10^9-10^{11} s^{-1}, and the transitions are easily observed provided their upper levels are excited and no $E1$ decay branch exists for the excited level.

Unlike the $2s_{1/2}$-$2p_{3/2}$ $E1$ transitions, the $2p_{1/2}$-$2p_{3/2}$ $M1$ or $E2$ transitions are generally only weakly excited by electron collisions. This was borne out by detailed modeling calculations we performed. Nevertheless, the $M1$ and $E2$ transitions are prominently observed in our spectral measurements, and their intensity is comparable to that of the $E1$ transitions measured earlier. To account for the observed intensity it was necessary to include indirect excitation processes in our model calculations. In particular, we show that excitation by radiative cascades, radiative capture, and ionization are highly effective, and dominate the excitation of the $M1$ and $E2$ lines. The line formation processes are thus similar to those observed to play the dominant role in the excitation of magnetic quadrupole ($M2$) transitions in neonlike ions [16], and magnetic octupole ($M3$) transitions in nickel-like [17] ions. These lines play an important role in plasma diagnostics, especially measurements of electron density and of nonequilibrium processes. In principle, the forbidden $n=2$ to $n=2$ lines in highly charged uranium could play a similar role in plasma diagnostics; plasma sources with sufficient temperature (>60 keV) to produce such highly charged ions, however, still need to be created.

The paper is structured as follows. In Sec. II, we present our theoretical estimates of the spectral line intensities. The production of highly charged uranium ions is described in Sec. III, followed by a description of the measurements and line identifications in Sec. IV. The spectral calibration and the results of our measurement are given in Sec. V. We end with a discussion of the results in Sec. VI.

II. PREDICTED LINE INTENSITIES

Generally, radiative rates for electric-dipole-forbidden $2p_{1/2}$-$2p_{3/2}$ decay are orders of magnitude smaller than the rates for allowed $2s_{1/2}$-$2p_{3/2}$ or $2s_{1/2}$-$2p_{1/2}$ decay. As a result, forbidden $2p_{1/2}$-$2p_{3/2}$ decay occurs only if $E1$ decay is impossible.

As an example, we consider the energy-level diagram of carbonlike U^{86+} in Fig. 1. We note that all excited levels with a $2s$ vacancy can decay via an $E1$ transition and, therefore, do not contribute to the spectra measured here. Those levels with a $2p_{1/2}$ vacancy can decay only via a dipole-forbidden transition. In particular, the level $(1s^2 2s^2 2p_{1/2} 2p_{3/2})_{J=1}$ decays via an $M1$ transition, while

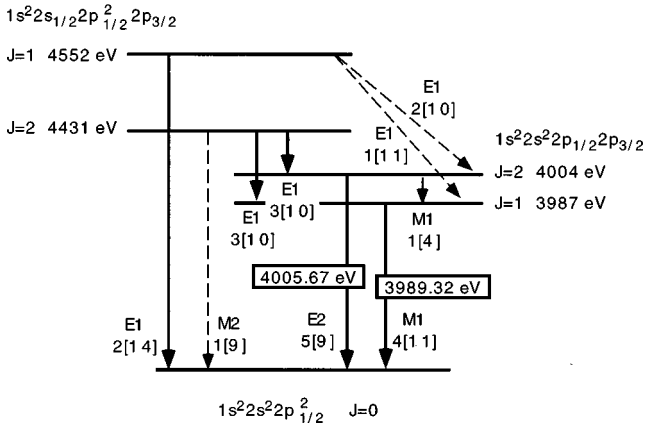

FIG. 1. Diagram of the lowest four excited levels in carbonlike U^{86+}. The dominant radiative decay branches from each level are indicated by solid arrows. The radiative decay rate denoted by $x[y]$ means $x\times 10^{y}$ s^{-1}. The measured energies of both $2p_{1/2}$-$2s_{1/2}$ transitions observed in the present study are given in framed boxes.

level $(1s^2 2s^2 2p_{1/2} 2p_{3/2})_{J=2}$ (in the absence of electron collisions) must decay via an $E2$ transition to the ground state. Hence we expect to see two $2p_{1/2}$-$2p_{3/2}$ transitions from carbonlike uranium in our spectrum. The situation is similar for all other ions, where an excited state can be formed from the ground level with a $2p_{3/2}$ optical electron and a $2p_{1/2}$ vacancy but no $2s_{1/2}$ vacancy, i.e., for all ions with charge state as high as boronlike U^{87+}.

Excited levels in charge states higher than boronlike U^{87+} require a $2s_{1/2}$ vacancy. Therefore, a $2s_{1/2}$-$2p_{3/2}$ $E1$ transition is possible, and takes precedence over a $2p_{1/2}$-$2p_{3/2}$ transition. An exception occurs, however, in the berylliumlike ion. Here the excited level $(1s^2 2s_{1/2} 2p_{3/2})_{J=2}$ is formed with a $2s$ vacancy. It deexcites via $2p_{1/2}$-$2p_{3/2}$ $M1$ decay because $2s_{1/2}$-$2p_{3/2}$ decay is not dipole allowed, and can only proceed via a dipole-forbidden $E2$ transition (cf. Fig. 2). Thus we expect to see $2p_{1/2}$-$2p_{3/2}$ decay in the berylliumlike ion, provided the $2p_{1/2}$-$2p_{3/2}$ $M1$ rate is faster or comparable to the $2s_{1/2}$-$2p_{3/2}$ $E2$ rate. This is indeed the

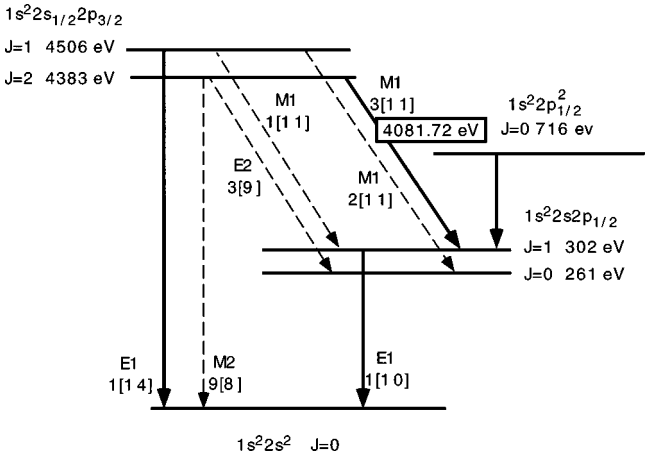

FIG. 2. Diagram of the lowest four excited levels in berylliumlike U^{88+}. The dominant radiative decay branches from each level are indicated by solid arrows. The radiative decay rate denoted by $x[y]$ means $x\times 10^{y}$ s^{-1}. The measured energy of the $2p_{1/2}$-$2p_{3/2}$ transition observed in the present study is given in a framed box.

case, as indicated by our calculations given in Fig. 2 and described below.

From inspection of the energy-level diagrams and the selection rules (or better, knowledge of the relative radiative decay rates), it is possible to understand which configurations might give rise to $2p_{1/2}$-$2p_{3/2}$ transitions. However, there is no obvious way to predict the strengths of the dipole-forbidden transitions without performing detailed calculations of all rates and processes involved.

In order to predict the radiative intensities of the uranium 2-2 transitions accurately, we have made two sets of detailed collisional-radiative calculations using atomic data generated with the Hebrew University-Lawrence Livermore atomic codes (HULLAC's) [18]. Our first model included all levels in all charge states, lithiumlike through neonlike uranium, with an optical electron in the $n=2$ shell. The model accounted for all radiative processes, including radiative cascades, and involved all electric and magnetic dipole and all electric and magnetic quadrupole transitions and all electron-impact excitation processes. We constructed a second model to predict the effects of indirect excitation processes, i.e., radiative cascades from the $n=3$ shell, radiative electron capture, and ionization of innershell electrons. These indirect processes are known to be important excitation processes, especially for dipole-forbidden transitions [16,17]. The second model included all levels in lithiumlike through fluorinelike uranium with an optical electron in the $n=2$ or 3 shell, radiative electron capture into the $n=2$ and 3 shells, and the ionization of $n=2$ electrons. Radiative electron capture and ionization link a given ion species to its neighboring ion species. In order to assure accurate predictions for the lithiumlike and neonlike transitions, we added the ground state level of heliumlike uranium and the first five lowest levels of sodiumlike uranium to the second model.

The model calculations show that the spectra of highly charged uranium ions from an electron-beam ion trap (EBIT) are produced in the low-collisional limit. This means that all excitations proceed from the ground level and are followed by radiative decay until they are back in the ground level. ''Ground level'' in the case of berylliumlike uranium includes not only the $1s^2 2s^2\ {}^1S_0$ true ground level but also the metastable level $1s^2 2s_{1/2} 2p_{1/2}\ {}^3P_0$, and in the case of oxygenlike uranium includes the metastable level $1s^2 2s^2 2p_{1/2}^2 2p_{3/2}^2\ J=0$ in addition to the $1s^2 2s^2 2p_{1/2}^2 2p_{3/2}^2$ $J=2$ ground level. In other words, any excited level decays fast enough via radiative deexcitation channels before any electron collision takes place. This is the result of the large radiative rates and correspondingly small electron-impact excitation rates. The $n=2\rightarrow 2$ radiative decay rates of interest are typically no less than about 10^{11}/s for magnetic-dipole transitions, and several order of magnitudes more for electric-dipole transitions. In contrast, the electron-impact excitation rates for these highly charged uranium ions range are less than a few per minute as a result of the smallness of the electron-impact excitation cross section (10^{-23}–10^{-25} cm^{-3} for 120-keV electrons) and an electron density of about 10^{12} cm^{-3} in our source.

Results from our two collisional-radiative model calculations for electron energies of 100 keV are presented in Table I for lithiumlike through nitrogenlike uranium, and in Table II for oxygenlike through neonlike uranium. Looking at the

TABLE I. Line intensities of the 2-2 transitions in U^{85+} through U^{89+} predicted by two collisional-radiative model calculations. $I_{n=2}$ denotes the intensity calculated from the balance of electron-impact excitation and radiative decay of electrons in the $n=2$ shell. $I_{n\leq 3}$ denotes the intensity calculated with an extended model that allows for excitation of electrons in the $n=2$ and 3 shells by electron-impact excitation, ionization of an electron from the $n=2$ shell, and radiative electron capture. Both calculations allow for radiative cascades via electric and magnetic dipole and electric and magnetic quadrupole transitions. An equal abundance of each ionization state (including heliumlike and sodiumlike uranium) is assumed in the extended model. The intensity of each line is normalized to that of the strongest line in a given charge state resulting from $n=2$ excitation, which is set equal to 100.0. Lines with relative intensities as low as 1.0 are listed. The assumed electron-beam energy is 120 keV. Also listed are the transition energies used in the atomic structure part of the modeling calculations.

Ion	Transition	Label	Type	Energy (eV)	$I_{n=2}$	$I_{n\leq 3}$	Fractional increase
U^{89+}	$(2p_{3/2})_{J=3/2}\rightarrow(2s_{1/2})_{J=1/2}$	Li-1	$E1$	4462.0	100.00	117.14	1.2
U^{88+}	$(2s_{1/2}2p_{3/2})_{J=1}\rightarrow(2s^2)_{J=0}$	Be-1	$E1$	4505.6	100.00	109.61	1.1
U^{88+}	$(2s_{1/2}2p_{3/2})_{J=2}\rightarrow(2s_{1/2}2p_{1/2})_{J=1}$	Be-2	$M1$	4081.1	0.70	4.40	6.3
U^{88+}	$(2p_{1/2}2p_{3/2})_{J=1}\rightarrow(2s_{1/2}2p_{1/2})_{J=0}$	Be-3	$E1$	4513.7	0.37	3.09	8.4
U^{88+}	$(2p_{1/2}2p_{3/2})_{J=1}\rightarrow(2s_{1/2}2p_{1/2})_{J=1}$	Be-4	$M1$	4473.1	0.19	1.53	8.0
U^{87+}	$(2s_{1/2}2p_{1/2}2p_{3/2})_{J=3/2}\rightarrow(2s^22p_{1/2})_{J=1/2}$	B-1	$E1$	4525.2	100.00	109.06	1.1
U^{87+}	$(2s_{1/2}2p_{1/2}2p_{1/2})_{J=3/2}\rightarrow(2s^22p_{1/2})_{J=1/2}$	B-2	$E1$	4525.3	52.31	57.50	1.1
U^{87+}	$(2s^22p_{3/2})_{J=3/2}\rightarrow(2s_{1/2}2p_{1/2}^2)_{J=1/2}$	B-3	$M1$	3678.1	1.53	9.72	6.4
U^{87+}	$(2s^22p_{3/2})_{J=3/2}\rightarrow(2s^22p_{1/2})_{J=1/2}$	B-4	$M1$	4086.1	1.07	6.75	6.3
U^{87+}	$(2s_{1/2}2p_{1/2}2p_{3/2})_{J=3/2}\rightarrow(2s^22p_{1/2})_{J=1/2}$	B-5	$E1$	4375.2	1.01	3.63	3.6
U^{86+}	$(2s_{1/2}2p^22p_{3/2})_{J=1}\rightarrow(2s^22p^2)_{J=0}$	C-1	$E1$	4552.4	100.00	116.56	1.2
U^{86+}	$(2s^22p_{1/2}2p_{3/2})_{J=2}\rightarrow(2s^22p^2)_{J=0}$	C-2	$E2$	4004.0	3.24	24.13	7.5
U^{86+}	$(2s^22p_{1/2}2p_{3/2})_{J=1}\rightarrow(2s^22p^2)_{J=0}$	C-3	$M1$	3987.3	0.30	16.65	55.5
U^{85+}	$(2s_{1/2}2p^22p_{3/2}^2)_{J=3/2}\rightarrow(2s^22p^22p_{3/2})_{J=3/2}$	N-1	$E1$	4593.5	100.00	118.78	1.2
U^{85+}	$(2s_{1/2}2p^22p_{3/2}^2)_{J=5/2}\rightarrow(2s^22p^22p_{3/2})_{J=3/2}$	N-2	$E1$	4443.8	25.88	52.65	2.0
U^{85+}	$(2s_{1/2}2p^22p_{3/2}^2)_{J=1/2}\rightarrow(2s^22p^22p_{3/2})_{J=3/2}$	N-3	$E1$	4591.6	26.10	34.78	1.3
U^{85+}	$(2s^22p_{1/2}2p_{3/2}^2)_{J=5/2}\rightarrow(2s^22p^22p_{3/2})_{J=3/2}$	N-4	$M1$	3963.1	3.46	25.01	7.2
U^{85+}	$(2s^22p_{1/2}2p_{3/2}^2)_{J=3/2}\rightarrow(2s^22p^22p_{3/2})_{J=3/2}$	N-5	$M1$	3941.9	0.90	14.04	15.6
U^{85+}	$(2s^22p_{1/2}2p_{3/2}^2)_{J=1/2}\rightarrow(2s^22p^22p_{3/2})_{J=3/2}$	N-6	$M1$	4041.1	0.88	7.64	8.7

relative line intensities predicted by the first model, which is based on direct electron-impact excitation within the $n=2$ shell only, we find that electric-dipole-forbidden $2p_{1/2}$-$2p_{3/2}$ transitions produce only very weak lines. The model calculations predict none of the forbidden lines with an intensity of more than a few percent of the intensity of the strongest dipole-allowed line for a given ionization state. Detection of dipole-forbidden lines would thus be very difficult given the low counting statistics of the measurements of the dipole-allowed $E1$ transitions reported in Ref. [8].

The picture changes dramatically when looking at the intensities predicted by our second model, which includes indirect excitation processes. Adding cascades from the $n=3$ levels, ionization of an electron from the $2s_{1/2}$ or $2p_{1/2}$ subshells, and radiative electron capture into excited configurations to the model greatly increases the relative intensity of the forbidden $2p_{1/2}-2p_{3/2}$ lines. Overall, each process contributes about one-third of the increase. The increase is close to an order of magnitude for most $M1$ and $E2$ transitions, as illustrated in Fig. 3. The strongest increases are seen for the carbonlike U^{86+} line labeled C-3 in Table I, and the fluorine-like U^{86+} line labeled F-2 in Table II. Their predicted intensities increased by factors of 55 and 21, respectively.

Because ionization and recombination link a given charge state to the abundance of a neighboring charge state, the line intensities computed with the second model are sensitive to the assumed abundance of the various charge states. The present results were obtained by assuming an equal abundance of all charge states. This is clearly incorrect, but the computed relative intensities do not depend strongly on this assumption.

While indirect excitation processes strongly enhance the forbidden lines, they have a comparatively small effect on the allowed $2s_{1/2}$-$2p_{3/2}$ lines. A look at Tables I and II shows that the enhancement ranges from about 10% to a factor of 2. As a consequence, the predicted intensities of the $E1$ do not change significantly, as illustrated in Fig. 4. The fact that indirect processes are the main contributors to the excitation of the forbidden 2-2 lines in highly charged ions, while contributing only marginally to the excitation of the allowed transitions, is very similar to the strong enhancement by indirect processes of the line intensity of the forbidden magnetic dipole line in heliumlike Ti^{20+} and of the magnetic quadrupole line in neonlike Ba^{46+} measured on an EBIT [16,19].

From our model calculations we expect to observe several strong $2p_{1/2}$-$2p_{3/2}$ lines in our spectra. The set comprises one strong line in U^{83+}, two in U^{84+}, one in U^{85+}, and two in U^{86+} (including the $E2$ line mentioned earlier). Several

TABLE II. Line intensities of the 2-2 transitions in U^{82+} through U^{84+} predicted by two collisional-radiative model calculations. The notation used is the same as used in Table I. An equal abundance of each ionization state (including heliumlike and sodiumlike uranium) is assumed in the extended model. The intensity of each line is normalized to that of the strongest line in a given charge state resulting from $n=2$ excitation, which is set equal to 100.0. Lines with relative intensities as low as 1.0 are listed. For neonlike U^{82+}, transitions only lines with relative intensity larger than 10.0 are listed. The assumed electron-beam energy is 120 keV. Also listed are the transition energies used in the atomic structure part of the modeling calculations.

Ion	Transition	Label	Type	Energy (eV)	$I_{n=2}$	$I_{n\leqslant 3}$	Fractional increase
U^{84+}	$(2s_{1/2}2p^2 2p^3_{3/2})_{J=2}\rightarrow(2s^2 2p^2 2p^2_{3/2})_{J=2}$	O-1	$E1$	4529.3	100.00	157.81	1.6
U^{84+}	$(2s_{1/2}2p^2 2p^3_{3/2})_{J=1}\rightarrow(2s^2 2p^2 2p^2_{3/2})_{J=2}$	O-2	$E1$	4647.6	71.80	95.31	1.3
U^{84+}	$(2s^2 2p_{1/2}2p^3_{3/2})_{J=2}\rightarrow(2s^2 2p^2 2p^2_{3/2})_{J=2}$	O-3	$M1$	3961.0	4.44	53.23	12.0
U^{84+}	$(2s_{1/2}2p^2 2p^3_{3/2})_{J=1}\rightarrow(2s^2 2p^2 2p^2_{3/2})_{J=0}$	O-4	$E1$	4562.0	26.47	35.16	1.3
U^{84+}	$(2s^2 2p_{1/2}2p^3_{3/2})_{J=1}\rightarrow(2s^2 2p^2 2p^2_{3/2})_{J=2}$	O-5	$M1$	3943.9	1.53	20.45	13.4
U^{84+}	$(2s^2 2p_{1/2}2p^3_{3/2})_{J=1}\rightarrow(2s^2 2p^2 2p^2_{3/2})_{J=0}$	O-6	$M1$	3858.3	0.57	7.68	13.4
U^{84+}	$(2s_{1/2}2p^2 2p^2_{3/2}3s_{1/2})_{J=2}\rightarrow(2s^2 2p^2 2p_{3/2}3s_{1/2})_{J=2}$	O-7	$E1$	4625.2	NA	5.70	NA
U^{84+}	$(2s_{1/2}2p^2 2p^2_{3/2}3d_{5/2})_{J=4}\rightarrow(2s^2 2p^2 2p_{3/2}3d_{5/2})_{J=4}$	O-8	$E1$	4625.2	NA	3.07	NA
U^{84+}	$(2s_{1/2}2p^2 2p^2_{3/2}3d_{3/2})_{J=4}\rightarrow(2s^2 2p^2 2p_{3/2}3d_{3/2})_{J=3}$	O-9	$E1$	4484.1	NA	1.77	NA
U^{83+}	$(2s_{1/2}2p^2 2p^4)_{J=1/2}\rightarrow(2s^2 2p^2 2p^3_{3/2})_{J=3/2}$	F-1	$E1$	4599.9	100.00	174.02	1.7
U^{83+}	$(2s^2 2p_{1/2}2p^4)_{J=1/2}\rightarrow(2s^2 2p^2 2p^3_{3/2})_{J=3/2}$	F-2	$M1$	3911.7	3.39	72.44	21.4
U^{83+}	$(2s_{1/2}2p^2 2p^3_{3/2}3s_{1/2})_{J=3/2}\rightarrow(2s^2 2p^2 2p^2_{3/2}3s_{1/2})_{J=5/2}$	F-3	$E1$	4669.5	NA	6.30	NA
U^{83+}	$(2s_{1/2}2p^2 2p^3_{3/2}3s_{1/2})_{J=3/2}\rightarrow(2s^2 2p^2 2p^2_{3/2}3s_{1/2})_{J=1/2}$	F-4	$E1$	4578.1	NA	2.91	NA
U^{83+}	$(2s_{1/2}2p^2 2p^3_{3/2}3d_{3/2})_{J=7/2}\rightarrow(2s^2 2p^2 2p^2_{3/2}3d_{3/2})_{J=7/2}$	F-5	$E1$	4531.6	NA	2.83	NA
U^{83+}	$(2s_{1/2}2p^2 2p^3_{3/2}3d_{5/2})_{J=7/2}\rightarrow(2s^2 2p^2 2p^2_{3/2}3d_{5/2})_{J=9/2}$	F-6	$E1$	4655.3	NA	2.40	NA
U^{83+}	$(2s^2 2p_{1/2}2p^3_{3/2}3p_{1/2})_{J=3/2}\rightarrow(2s^2 2p^2 2p^2_{3/2}3p_{1/2})_{J=3/2}$	F-7	$M1$	4194.8	NA	1.90	NA
U^{83+}	$(2s_{1/2}2p^2 2p^3_{3/2}3s_{1/2})_{J=3/2}\rightarrow(2s^2 2p^2 2p^2_{3/2}3s_{1/2})_{J=3/2}$	F-8	$E1$	4654.4	NA	1.82	NA
U^{82+}	$(2s_{1/2}2p^2 2p^4 3s_{1/2})_{J=1}\rightarrow(2s^2 2p^2 2p^3_{3/2}3s_{1/2})_{J=2}$	Ne-1	$E1$	4598.6	NA	100.00	NA
U^{82+}	$(2s_{1/2}2p^2 2p^4 3s_{1/2})_{J=0}\rightarrow(2s^2 2p^2 2p^3_{3/2}3s_{1/2})_{J=1}$	Ne-2	$E1$	4639.2	NA	90.97	NA
U^{82+}	$(2s^2 2p_{1/2}2p^4 3s_{1/2})_{J=0}\rightarrow(2s^2 2p^2 2p^3_{3/2}3s_{1/2})_{J=1}$	Ne-3	$E1$	3892.7	NA	34.78	NA
U^{82+}	$(2s^2 2p_{1/2}2p^4 3p_{1/2})_{J=0}\rightarrow(2s^2 2p^2 2p^3_{3/2}3s_{1/2})_{J=1}$	Ne-4	$E1$	4170.1	NA	25.16	NA
U^{82+}	$(2s_{1/2}2p^2 2p^4 3s_{1/2})_{J=1}\rightarrow(2s^2 2p^2 2p^3_{3/2}3s_{1/2})_{J=1}$	Ne-5	$E1$	4586.8	NA	20.22	NA
U^{82+}	$(2s_{1/2}2p^2 2p^4 3d_{3/2})_{J=2}\rightarrow(2s^2 2p^2 2p^3_{3/2}3d_{1/2})_{J=3}$	Ne-6	$E1$	4607.7	NA	18.74	NA
U^{82+}	$(2s_{1/2}2p^2 2p^4 3d_{5/2})_{J=2}\rightarrow(2s^2 2p^2 2p^3_{3/2}3d_{5/2})_{J=2}$	Ne-7	$E1$	4612.6	NA	17.29	NA
U^{82+}	$(2s_{1/2}2p^2 2p^4 3d_{5/2})_{J=2}\rightarrow(2s^2 2p^2 2p^3_{3/2}3d_{5/2})_{J=3}$	Ne-8	$E1$	4599.7	NA	14.12	NA
U^{82+}	$(2s^2 2p_{1/2}2p^4 3p_{1/2})_{J=0}\rightarrow(2s^2 2p^2 2p^3_{3/2}3p_{1/2})_{J=1}$	Ne-9	$E1$	3966.3	NA	12.82	NA
U^{82+}	$(2s_{1/2}2p^2 2p^4 3d_{5/2})_{J=2}\rightarrow(2s^2 2p^2 2p^3_{3/2}3d_{5/2})_{J=1}$	Ne-10	$E1$	4563.7	NA	12.56	NA

weaker lines, including one in berylliumlike U^{88+}, are also predicted by our model.

III. PRODUCTION OF HIGHLY CHARGED URANIUM IONS

The production and spectral analysis was performed at the high-energy electron-beam ion trap, dubbed SuperEBIT, at the Lawrence Livermore National Laboratory. The setup was similar to that used in our measurements of the $2s_{1/2}$-$2p_{3/2}$ transitions in highly charged uranium [8] and thorium [4] reported earlier.

In order to produce highly charged uranium ions, the trap was first filled with singly charged uranium ions injected from a metal vapor arc source. These ions are then successively ionized in the interaction with a 165-mA, 60-μm-diameter electron beam at an energy of either 105 or 132 keV. Modeling calculations show that it takes less than one second to produce substantial amounts of uranium ions with vacancies in the L shell, i.e., to produce ions with charges $q=83+$ through $89+$. An equilibrium charge distribution is reached after about 4 or 5 s, as discussed in Ref. [4] for the case of thorium. The ions were kept in the trap for about half of 1 min. Then the trap was emptied and refilled with new ions from the metal vapor arc source.

The x-ray emission from the ions was monitored via ports that provided direct line-of-sight access to the trap. A high-purity 50.7-mm-diameter, 18.9-mm-deep Ge detector was used to provide a broadband x-ray survey of the x-ray emission. A representative spectrum obtained with the Ge detector is shown in Fig. 5. Unlike the spectra recorded in beam-foil measurements, where ions move at relativistic speeds, the SuperEBIT spectra record the actual x-ray energy emitted by the ions, and no Doppler-shift corrections are necessary. The spectrum shows the two features corresponding to the location of the $1s^2$-$1s2p_{1/2}$ and $1s^2$-$1s2p_{3/2}$ K-shell emission at 96 and 100 keV, respectively. The spectrum also shows prominent radiative recombination lines. Unlike in plasmas with a Maxwellian electron distribution where radiative recombination photons form a continuum, radiative re-

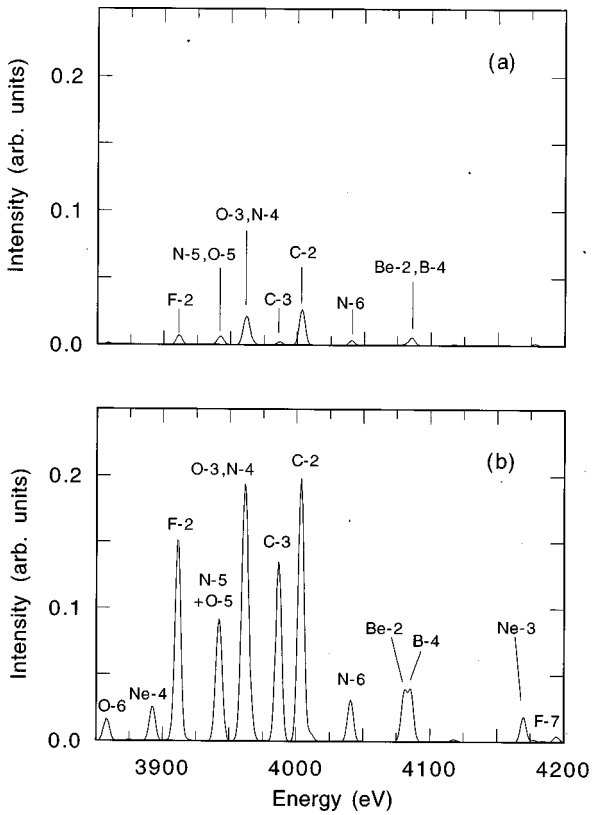

FIG. 3. Intensities of the $2p_{1/2}$-$2p_{3/2}$ electric-dipole-forbidden transitions in U^{82+} through U^{89+} predicted by collisonal-radiative calculations: (a) model calculations including only electron excitation and radiative cascades among the $n=2$ and the ground level; (b) model calculations including electron excitation and radiative cascades among the $n=3$, $n=2$, and ground level as well as electron capture into excited states and ionization of a $2s$ or $2p$ electron. Lines are labeled by the ionization stage of the emitting ion using the notation of Tables I and II.

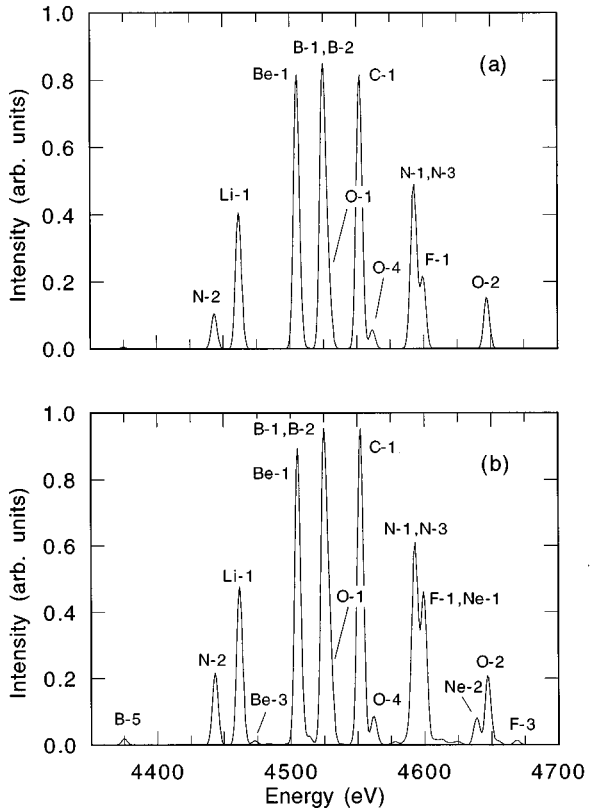

FIG. 4. Intensities of the $2s_{1/2}$-$2p_{3/2}$ electric-dipole-allowed transitions in U^{82+} through U^{89+} predicted by collisonal-radiative calculations: (a) model calculations including only electron excitation and radiative cascades among the $n=2$ and the ground level; (b) model calculations including electron excitation and radiative cascades among the $n=3$, $n=2$, and ground level as well as electron capture into excited states and ionization of a $2s$ or $2p$ electron. Lines are labeled by the ionization stage of the emitting ion using the notation of Tables I and II.

combination photons form distinct lines in an EBIT as a result of the monoenergetic electron beam. Because the energy of the radiative recombination x rays equals the sum of the energy of the captured electron plus the ionization energy of the recombined ions, features produced by radiative recombination lie in energy well above that of characteristic and bremsstrahlung x rays and are thus well resolved. In particular, the features produced by the radiative capture of beam electrons into the $n=2$, 3, 4, and 5 shell are readily identified. Photons produced by capture into yet higher shells are unresolved and form a smooth transition with the bremsstrahlung continuum that ends at 105 keV, the energy of the electron beam for this particular measurement.

Similar to the splitting of the K-shell line emission, the recombination peak into the $n=2$ shell is split by the spin-orbit interaction into two components: capture into $j=\frac{3}{2}$ levels and capture into $j=\frac{1}{2}$ levels. All charge states higher than neonlike have a vacancy in the $2p_{3/2}$ subshell and thus can, in principle, contribute to the $j=\frac{3}{2}$ recombination feature. By contrast, only charge states higher than carbonlike with a vacancy in the $2p_{1/2}$ or $2s_{1/2}$ subshell can contribute to the $j=\frac{1}{2}$ recombination feature. The relative ratio of the $j=\frac{1}{2}-\frac{3}{2}$ feature, therefore, presents a measure of the charge balance.

IV. SPECTRAL MEASUREMENTS AND LINE IDENTIFICATION

The 2-2 line emission was resolved with a high-resolution von Hámos-type crystal spectrometer [20]. The spectrometer used a $120\times50\times0.25$-mm^3 LiF(200) crystal with a lattice spacing $2d=4.027$ Å bent to a 30-cm radius of curvature. The diffracted x rays were recorded with a gas-filled proportional counter with a $10\times3\times0.4$-cm^3 active volume. The working gas consisted of 70% xenon and 30% methane at 1.2-atm overpressure. The resolving power of the setup was about $\lambda/\Delta\lambda=2200$, and was mainly limited by the 270-μm spatial resolving power of the detector. This setup was identical to that used in Ref. [4] for measuring the thorium $E1$ emission.

A spectrum of the $2p_{3/2}\rightarrow2p_{1/2}$ transitions is shown in Fig. 6. The energy range covered by the measurements extended from 3850 to 4200 eV. A total of eight distinct features were noted in the observed spectra. Following our modeling calculations, we proceeded to identify ten transitions in the seven charge states between U^{83+} through U^{88+} as forming the eight features in the spectrum. These are labeled in Fig. 6 using the notation of Tables I and II. In particular, we identified the strongest of the predicted $M1$ transitions in U^{83+}, the strongest two of the predicted $M1$

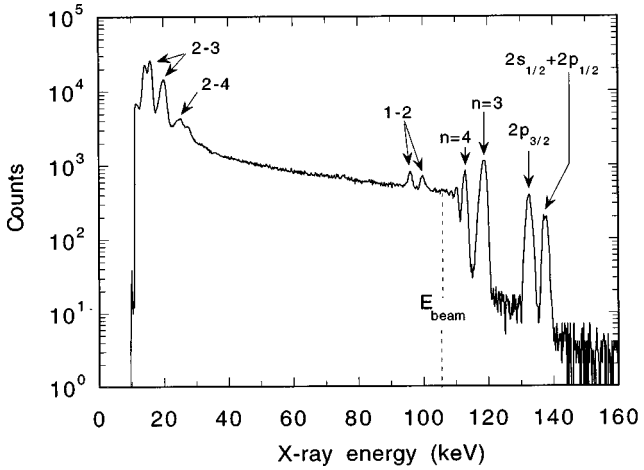

FIG. 5. Hard x-ray-emission spectrum from highly charged uranium ions in SuperEBIT. The spectrum produced by a 105-keV, 165-mA electron beam was observed with a high-purity Ge detector. Features below the beam energy sit on top of a bremsstrahlung background and are produced by electron-impact excitation. The $2s_{1/2}$, $2p_{1/2}\rightarrow 1s_{1/2}$ and $2p_{3/2}\rightarrow 1s_{1/2}$ $K\alpha$ transitions are seen near 96 and 100 keV, respectively; the L-shell transitions are prominent below about 32 keV. The bremsstrahlung background ceases at the energy of the electron beam. Features above this energy arise from radiative electron capture into the particular n shell indicated. Capture into the $n=2$ shell produces two distict features indicative of the angular momentum of the capturing level, i.e., $j=\frac{1}{2}$ for capture into $2s_{1/2}$ and $2p_{1/2}$ levels or $j=\frac{3}{2}$ for capture into $2p_{3/2}$.

transitions in U^{84+}, the strongest three of the predicted $M1$ transitions in U^{85+}, the strongest of the predicted $M1$ transitions in U^{86+}, the second strongest of the predicted $M1$ transitions in U^{87+}, and the strongest of the predicted $M1$ transitions in U^{88+}. We also identified the strong $E2$ transition predicted in U^{86+}. The strongest of the predicted $M1$ transitions in U^{87+} was not identified, because it fell outside our spectral range. Two of the observed features consist of a blend of two lines each. The blend could be readily resolved by using least-squares fits of two Gaussian-shaped lines.

While the modeling predictions aided the identification of the spectral lines, the observations validated the modeling predictions. The count rate, i.e., the spectral line intensity we observed in the $2p_{1/2}$-$2p_{3/2}$ spectrum per unit time is about 50% of that we observed earlier in our measurements [4,8] of the $2s_{1/2}$-$2p_{3/2}$ spectra. Our modeling calculations indicated that the non-$E1$ transitions are primarily populated by indirect excitation processes. Inclusion of indirect excitation processes enhanced the relative intensities of the forbidden transitions from a few percent to about 20–50 % of that of the allowed transitions. The present observations thus agree on a broad scale with the modeling predictions that include indirect processes.

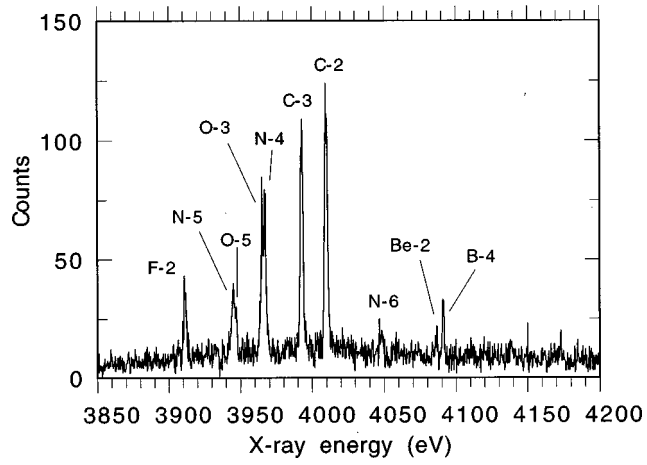

FIG. 6. Crystal-spectrometer spectrum of the $2p_{1/2}-2p_{3/2}$ electric-dipole-forbidden transitions in U^{83+} through U^{88+}. The lines are labeled by the ionization stage of the emitting ion using the notation of Tables I and II.

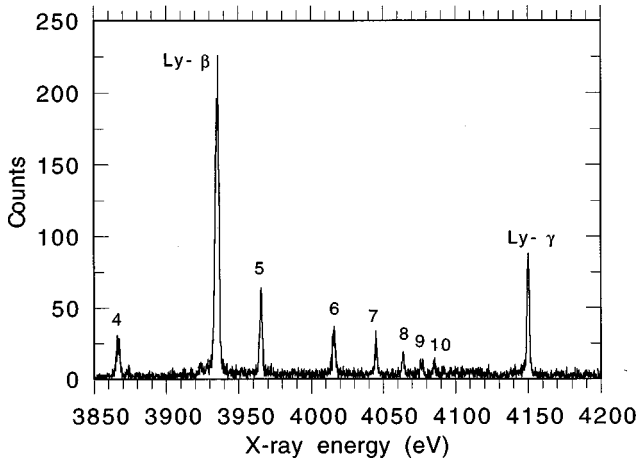

FIG. 7. Spectrum of the K-shell x rays from hydrogenic and heliumlike argon. The Ly-β and Ly-γ transitions in hydrogenlike argon were used to calibrate the absolute energy and dispersion of the spectrometer. The heliumlike lines are labeled by the principal quantum number of the upper level. The line from $n=4$ (He-δ) is at the edge of the spectrometer sensitivity and is partially cut off.

V. SPECTRAL CALIBRATION

Similar to our earlier measurements of the thorium $E1$ spectra [4], which were situated in the same wavelength range, transitions in hydrogenlike argon were used to calibrate the $2p_{1/2}$-$2p_{3/2}$ spectrum of the uranium. We recorded spectra of the Ly-β and Ly-γ lines spanning a spectral region from about 3850–4200 eV. The argon spectra were recorded in an alternating fashion with the uranium spectra using the same beam energy and beam current. On average 1 h was spent recording an argon spectrum. This was followed by the recording of a uranium spectrum for 4 h. The recording times for argon lines were significantly shorter because of the higher intensity of the Lyman lines compared to the uranium $2p_{1/2}-2p_{3/2}$ transitions. A spectrum showing the hydrogenlike argon transitions is shown in Fig. 7. Data were collected during two independent measurement periods, which were three months appart.

As discussed in Ref. [4] the lines of hydrogenlike argon represent a good choice for calibration because their energies are theoretically well known. The energy of the $1s$ ground state of hydrogenlike argon has been calculated, for example, by Garcia and Mack [21], Erickson [22], and Johnson and Soff [23]. These values differ by no more than 0.0143 eV.

Following the discussion in Ref. [4], we set the energies of the unresolved components of the Ly-β and Ly-γ lines

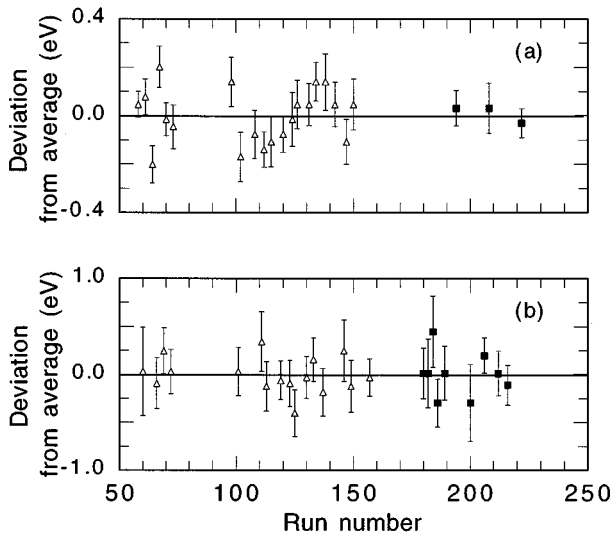

FIG. 8. Time dependence of the observed line positions throughout the measurement period. (a) Ly-β line of hydrogenlike Ar^{17+} used as one of the reference lines. (b) Line C-2 of carbonlike U^{86+}. Each run lasted about 1–2 h in the case of argon, and 3–4 h in the case of uranium. The open triangles and solid squares denote results from two different run periods, which were three months apart. Uncertainty limits are solely based on counting statistics.

equal to 3935.19 and 4150.11 eV, respectively, and assume an uncertainty of 0.06 eV for these reference energies. This uncertainty takes into account the uncertainty in the relative intensities of the individual components of the unresolved reference lines.

We recorded 25 separate spectra of uranium and almost as many spectra of argon. A plot of the position of the $2p$-$2p$ transition in carbonlike U^{85+} and of the Ly-β line in Ar^{17+} as a function of time is given in Fig. 8. Error bars indicate statistical uncertainties only. The measured line positions were highly reproducible, typically within about a tenth of an eV. Drifts in the spectrometer and the response of the electronics were not noted, and neither were drifts in the source. Systematic uncertainties arising from these effects were thus excluded.

The energies of the uranium $2p_{1/2}$-$2p_{3/2}$ transitions are listed in Table III. The uncertainties in the measured energies represent 1σ error limits given by the quadrature sum of five contributions: the statistical uncertainties of the positions of the uranium lines, the statistical uncertainties of the positions of the calibration lines, the systematic uncertainties associated with the uncertainties in the wavelengths of the hydrogenlike calibration lines, uncertainties arising from nonlinearities in the detector response, and uncertainties caused by blending with other lines. An overview of the individual contributions to the overall measurement uncertainty of the carbonlike $2p_{1/2}$-$2p_{3/2}$ transition C-3 is given in Table IV. The overall statistical uncertainty in the measured line positions from all runs is 0.025 eV. The statistical uncertainty in the line positions of the calibration lines adds 0.060 eV. In addition, there is a 0.06-eV contribution from the uncertainty in the absolute energy of the calibration lines, as discussed above. Finally, there is a 0.10-eV contribution from the integral nonlinearity in the detector response. The value of this contribution corresponds to the measured spatial linearity of 20 μm for the detector employed in our spectrometer, and represents a very conservative estimate, as shown in Ref. [24]. There is no contribution from blending with other lines. Adding all contributions in quadrature gives an uncertainty of 0.13 eV with which the energy of the carbonlike transition C-3 was determined. This uncertainty corresponds to a measurement accuracy of better than 35 ppm. The uncertainties in the measured energies of the other nine transitions are of comparable magnitude. The total error varies from ± 0.13 to ± 0.33 eV. The two lines N-4 and O-3 have the largest uncertainties because of a 0.25-eV contribution from the uncertainty associated with resolving the two lines from each other

TABLE IV. Contributions to the uncertainty in the measured transition energy of line C-2 in carbonlike U^{86+}.

Source	Magnitude (eV)
Position of uranium line	0.025
Dispersion	0.060
Energy of reference lines	0.060
Detector linearity	0.100
Blending with other lines	0.000

TABLE III. Summary of the measured energies of the $2p_{1/2}$-$2p_{3/2}$ transitions in U^{83+} through U^{88+} (in eV). The given uncertainties represent 1σ confidence limits. E_{theory}-E_{expt} expresses the differences with the theoretical values given in Tables I and II.

Ion	Key	Transition	E_{expt}	E_{theory}-E_{expt}
U^{88+}	Be-2	$(2s_{1/2}2p_{3/2})_{J=2}\rightarrow(2s_{1/2}2p_{1/2})_{J=1}$	4081.72 ± 0.27	-0.6
U^{87+}	B-4	$(2s^2 2p_{3/2})_{J=3/2}\rightarrow(2s^2 2p_{1/2})_{J=1/2}$	4087.02 ± 0.17	-0.9
U^{86+}	C-2	$(2s^2 2p_{1/2}2p_{3/2})_{J=2}\rightarrow(2s^2 2p^2)_{J=0}$	4005.67 ± 0.13	-1.7
U^{86+}	C-3	$(2s^2 2p_{1/2}2p_{3/2})_{J=1}\rightarrow(2s^2 2p^2)_{J=0}$	3989.32 ± 0.13	-2.0
U^{85+}	N-4	$(2s^2 2p_{1/2}2p_{3/2}^2)_{J=5/2}\rightarrow(2s^2 2p^2 2p_{3/2})_{J=3/2}$	3964.88 ± 0.15	-1.8
U^{85+}	N-5	$(2s^2 2p_{1/2}2p_{3/2}^2)_{J=3/2}\rightarrow(2s^2 2p^2 2p_{3/2})_{J=3/2}$	3943.65 ± 0.33	-1.8
U^{85+}	N-6	$(2s^2 2p_{1/2}2p_{3/2}^2)_{J=1/2}\rightarrow(2s^2 2p^2 2p_{3/2})_{J=3/2}$	4042.40 ± 0.24	-1.3
U^{84+}	O-3	$(2s^2 2p_{1/2}2p_{3/2}^3)_{J=2}\rightarrow(2s^2 2p^2 2p_{3/2}^2)_{J=2}$	3962.77 ± 0.15	-1.8
U^{84+}	O-5	$(2s^2 2p_{1/2}2p_{3/2}^3)_{J=1}\rightarrow(2s^2 2p^2 2p_{3/2}^2)_{J=2}$	3945.34 ± 0.33	-1.4
U^{83+}	F-2	$(2s_{1/2}2p^2 2p^4)_{J=1/2}\rightarrow(2s^2 2p^2 2p_{3/2}^3)_{J=3/2}$	3913.54 ± 0.16	-1.8

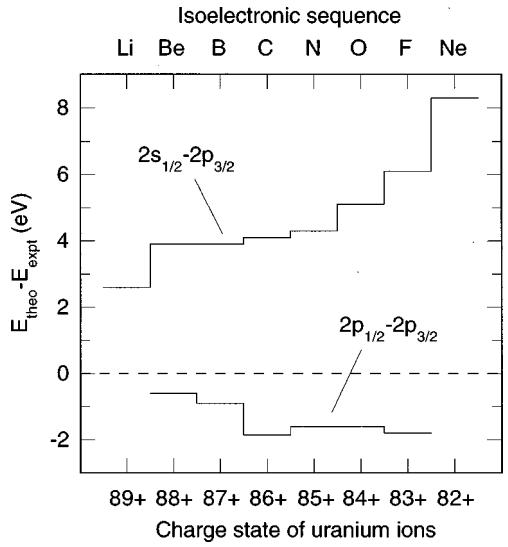

FIG. 9. Average difference between calculated (cf. Tables I and II) and measured transition energies for each charge state of uranium. The experimental values for the $2s_{1/2}$-$2p_{3/2}$ electric-dipole-allowed transitions in U^{82+} through U^{89+} are taken from Ref. [8]; those for the $2p_{1/2}$-$2p_{3/2}$ electric-dipole-forbidden transitions in U^{82+} through U^{88+} are from the present measurement.

using least-square fitting procedures. The uncertainty of lines Be-2 and N-6 is high because the lines represent the two weakest lines identified.

VI. DISCUSSION AND COMPARISON WITH THEORY

A comparison of the measured $2s_{1/2}$-$2p_{3/2}$ transition energies in highly charged thorium and uranium [4,8] had shown systematic differences with multiconfiguration Dirac-Fock (MCDF) calculations. There were two reasons for the differences. First, the calculations of the QED contributions using the standard codes [25,26] are only approximations. The inaccuracy in the QED contributions was found to be 2.1 eV for the 2-2 uranium transitions [8]. Second, electron correlations will not be fully accounted for, if only a limited amount of configurations is included. The underaccounting of correlation contributions was insignificant for the $2s_{1/2}$-$2p_{3/2}$ transition L-1 in lithiumlike uranium, but added about 6 eV to the difference between measurement and calculation to the neonlike transition Ne-2.

The transition energies calculated with the HULLAC differ from the measured values by almost identical amounts as those calculated with MCDF methods in Ref. [8]. The differences between the $2s_{1/2}$-$2p_{3/2}$ $E1$ transition energies in uranium measured in Ref. [8] and our HULLAC calculations are shown in Fig. 9 as a function of charge state. The average difference is shown for those charge states for which more than one transition was measured. The figure illustrates that the differences increases from 2.6 eV for L-1 to 8.3 eV for Ne-2.

The difference between the transition energies calculated with the HULLAC and the measured energies of the forbidden $M1$ and $E2$ lines is also shown in Fig. 9. The observed differences go into the opposite direction as those for the allowed $E1$ lines. While the theoretical predictions for the allowed transition are larger than measured, they are smaller than measured for the forbidden transitions. The magnitude of the differences increases from 0.6 eV for berylliumlike U^{88+} to 1.8 eV in fluorinelike U^{83+}. This is a smaller increase than that found for the allowed transitions.

New methods for calculating the atomic structure of highly charged ions were implemented recently by Johnson, Sapirstein, and Cheng [9], Cheng and Chen [10], Safronova, Johnson, and Safronova [11], and Chen and Cheng [12]. The various approaches used by these authors yielded good agreement with the measurements of the $2s_{1/2}$-$2p_{3/2}$ transitions with differences ranging from about 0.1–0.6 eV. To our knowledge, no such calculations have yet been carried out for the $2p_{1/2}$-$2p_{3/2}$ transitions, as no experimental measurements were available for comparison. Our present measurements now provide the experimental benchmarks for testing such advanced calculations in a new way. As illustrated by Fig. 9, the systematics followed by the $2p_{1/2}$-$2p_{3/2}$ transitions is different from that followed by the $2s_{1/2}$-$2p_{3/2}$ transitions, intimating that the forbidden lines test different aspects of the calculations than the allowed lines. The measurement of forbidden lines is thus complementary to the measurement of allowed transitions for guiding the development of advanced structure calculations in the strong-field limit.

The need for more accurate calculations of the transition energies of very highly charged ions was illustrated recently in an attempted measurement of the $1s2p\ ^3P_2 \rightarrow 1s2s\ ^3S_1$ in heliumlike U^{90+} [27]. This transition was predicted to produce a line at 4510.01 eV [28]. A feature with the appropriate energy (4510.05 ± 0.24 eV) was indeed observed. However, there were doubts as to the true identity of the observed feature, because of the possibility that the feature might correspond to, or blend with, a 2-2 transition in berylliumlike U^{88+}. The latter, corresponding to line Be-3 in Table I, was predicted to be more intense than the heliumlike line [27] but not identified at the position of 4513.7 eV predicted by the MCDF calculations.

Although the $2p_{1/2}$-$2p_{3/2}$ transitions do not involve $2s$ electrons, their energies are nevertheless affected by a net QED contribution of more than 2 eV. In fact, Blundell, Johnson, and Sapirstein [29] estimated 2.15 eV for the QED contribution to the $2p_{1/2}$-$2p_{3/2}$ transition in lithiumlike U^{89+}. A more detailed accounting was given by Indelicato and Desclaux [30]. They explicitly calculated various contributions to both the self-energy and vacuum polarization affecting the $1s^2 2p_{1/2}$ and $1s^2 2p_{3/2}$ levels in U^{89+}. They found that the $2p_{1/2}$-$2p_{3/2}$ transition is affected by a net QED contribution of 2.44 eV. Most interestingly, their calculation showed that the net QED contribution is by a wide margin due to the differences in the vacuum polarization terms, i.e., 2.29 eV out of 2.44 eV, as the self-energy is nearly the same for both levels [30]. An even higher net difference of the vacuum polarization terms was obtained by Persson *et al.* [31]. They calculated 2.60 eV. Although no *ab initio* calculations exist for the QED contributions to any of the $2p_{1/2}$-$2p_{3/2}$ transitions in the lower charge states of uranium, we can make the assumption that the net contribution is also about 2.5 eV for the forbidden transitions in the charge states lower than U^{89+}. Our 0.13-eV measurement of the $2p_{1/2}$-$2p_{3/2}$ transition energy in carbonlike U^{86+}, therefore, represents a 5% measurement of the net QED contribution of

the C-3 transition. This parallels the 6% accuracy with which the $1s_{1/2}$-$2p_{3/2}$ transition energy has been measured so far in hydrogenlike U^{91+} [7]. The present measurements thus also represent accurate benchmarks for testing QED calculations, especially vacuum polarization calculations. In principle, if the non-QED energies were known with high accuracy, our measurements would allow to distinguish between different calculations of the vacuum polarization energy term. The present measurements thus provide not only a testbed for advanced methods of calculating the non-QED energies, such as RMBPT, but also *ab initio* methods for calculating the QED contributions.

ACKNOWLEDGMENTS

This work was performed under the auspices of the Department of Energy by Lawrence Livermore National Laboratory under Contract No. W-7405-ENG-48 and supported in part by the Division of Chemical Physics in the Office of Basic Energy Sciences of the Department of Energy.

[1] P. Beiersdorfer, M. H. Chen, R. E. Marrs, and M. A. Levine, Phys. Rev. A **41**, 3453 (1990).
[2] P. Beiersdorfer, S. R. Elliott, J. Crespo López-Urrutia, and K. Widmann, Nucl. Phys. A **626**, 357 (1997).
[3] P. Beiersdorfer, Nucl. Instrum. Methods Phys. Res. B **99**, 114 (1995).
[4] P. Beiersdorfer, A. Osterheld, S. R. Elliott, M. H. Chen, D. Knapp, and K. Reed, Phys. Rev. A **52**, 2693 (1995).
[5] J. Schweppe, A. Belkacem, L. Blumenfeld, N. Claytor, B. Feinberg, H. Gould, V. E. Kostroun, L. Levy, S. Misawa, J. R. Mowat, and M. H. Prior, Phys. Rev. Lett. **66**, 1434 (1991).
[6] P. Beiersdorfer, A. Osterheld, J. Scofield, J. Crespo López-Urrutia, and K. Widmann, Phys. Rev. Lett. **80**, 3022 (1998).
[7] H. F. Beyer, G. Menzel, D. Liesen, A. Gallus, F. Bosch, R. Deslattes, P. Indelicato, Th. Stöhlker, O. Klepper, R. Moshammer, F. Nolden, H. Eickhoff, B. Franzke, and M. Steck, Z. Phys. D **35**, 169 (1995).
[8] P. Beiersdorfer, D. Knapp, R. E. Marrs, S. R. Elliott, and M. H. Chen, Phys. Rev. Lett. **71**, 3939 (1993).
[9] W. R. Johnson, J. Sapirstein, and K. T. Cheng, Phys. Rev. A **51**, 297 (1995).
[10] K. T. Cheng and M. H. Chen, Phys. Rev. A **53**, 2206 (1996).
[11] M. S. Safronova, W. R. Johnson, and U. I. Safronova, Phys. Rev. A **53**, 4036 (1997).
[12] M. H. Chen and K. T. Cheng, Phys. Rev. A **55**, 166 (1997).
[13] B. Edlén, Phys. Scr. **28**, 51 (1983).
[14] B. Denne, E. Hinnov, J. Ramette, and B. Saoutic, Phys. Rev. A **40**, 1488 (1989).
[15] R. Myrnäs, C. Jupén, G. Miecznik, I. Martinson, and B. Denne-Hinnov, Phys. Scr. **49**, 429 (1994).
[16] P. Beiersdorfer, A. L. Osterheld, M. H. Chen, J. R. Henderson, D. A. Knapp, M. A. Levine, R. E. Marrs, K. J. Reed, M. B. Schneider, and D. A. Vogel, Phys. Rev. Lett. **65**, 1995 (1990).
[17] P. Beiersdorfer, A. L. Osterheld, J. Scofield, B. Wargelin, and R. E. Marrs, Phys. Rev. Lett. **67**, 2272 (1991).
[18] A. Bar-Shalom, M. Klapisch, and J. Oreg, Phys. Rev. A **38**, 1773 (1988).
[19] S. Chantrenne, P. Beiersdorfer, R. Cauble, and M. B. Schneider, Phys. Rev. Lett. **69**, 265 (1992).
[20] P. Beiersdorfer, R. E. Marrs, J. R. Henderson, D. A. Knapp, M. A. Levine, D. B. Platt, M. B. Schneider, D. A. Vogel, and K. L. Wong, Rev. Sci. Instrum. **61**, 2338 (1990).
[21] J. D. Garcia and J. E. Mack, J. Opt. Soc. Am. **55**, 654 (1965).
[22] G. W. Erickson, J. Phys. Chem. Ref. Data **6**, 831 (1977).
[23] W. R. Johnson and G. Soff, At. Data Nucl. Data Tables **33**, 405 (1985).
[24] D. Vogel, P. Beiersdorfer, V. Decaux, and K. Widmann, Rev. Sci. Instrum. **66**, 776 (1995).
[25] I. P. Grant, B. J. McKenzie, P. H. Norrington, D. F. Mayers, and N. C. Pyper, Comput. Phys. Commun. **21**, 207 (1980).
[26] K. G. Dyall, I. P. Grant, C. T. Johnson, F. A. Parpia, and E. P. Plummer, Comput. Phys. Commun. **55**, 425 (1989).
[27] P. Beiersdorfer, S. R. Elliott, A. L. Osterheld, Th. Stöhlker, J. Autrey, G. V. Brown, A. J. Smith, and K. Widmann, Phys. Rev. A **53**, 4000 (1996).
[28] G. W. F. Drake, Can. J. Phys. **66**, 586 (1988).
[29] S. A. Blundell, W. R. Johnson, and J. Sapirstein, Phys. Rev. A **41**, 1698 (1990).
[30] P. Indelicato and J. P. Desclaux, Phys. Rev. A **42**, 5139 (1990).
[31] H. P. Persson, I. Lindgren, S. Salomonson, and P. Sunnergren, Phys. Rev. A **48**, 2772 (1993).